Absorption and multi-phonon quenching in nanocrystal doped SiO₂ fibers

MICHAEL STEINKE,[1,*] **SIMON SPELTHANN,**[1,2] **AXEL RÜHL,**[3] **AND DETLEV RISTAU**[1,4]

[1]*Leibniz Universität Hannover, Institut für Quantenoptik, Welfengarten 1, 30167 Hannover, Germany*
[2]*Laser Zentrum Hannover e.V., Hollerithallee 8, 30419 Hannover, Germany*
[3]*Leibniz Universität Hannover, QUEST-Leibniz-Research School, Institut für Quantenoptik, Callinstrasse 36, 30167 Hannover, Germany*
[4]*Cluster of Excellence PhoenixD (Photonics, Optics, and Engineering - Innovation Across Disciplines), Hannover, Germany*
[*]michael.steinke@hitec.uni-hannover.de

Abstract: SiO₂ fibers doped with rare-earth-doped nanocrystals are promising to overcome the strong SiO₂ multi-phonon quenching and could yield novel laser gain materials. So far, no attention has been paid to the question how well the nanocrystals can suppress the quenching depending on the properties of the SiO₂ host glass. Here, a novel analytical model was applied to study the impact of the glass purity and composition on the quenching efficiency. Only a few experimentally accessible material and design parameters are required to compute the average quenching rate inside the nanocrystals. It is demonstrated that sufficiently low levels of quenching can only be expected for SiO₂ free of impurities or dopants that increase the multi-phonon absorption. This indicates that high-purity aluminosilicate glasses, in contrast to phosphosilicate and borosilicate glasses, are ideal hosts.

1. Introduction

Optical glass fibers are a key technology of modern times. In particular, rare-earth (RE) doped fibers in corresponding fiber lasers are essential for material processing [1], for biomedicine [2], for telecommunication [3] or for fundamental research [4]. Despite the technological evolution of alternative glasses such as ZBLAN [5,6], SiO₂ remains one of the best host glasses for various fundamental (e.g. high thermal robustness) and technological (e.g. low loss splicing) reasons. However, the operation regime of RE doped SiO₂ fibers is restricted to a narrow spectral window in the IR from around $1\,\mu$m to $2\,\mu$m. Potential transitions of RE ions in the visible (VIS) regime, for example of Pr^{3+} or of Er^{3+}, cannot be addressed because the lifetimes of the relevant electronic states are quenched by the high SiO₂ phonon energy of around $1100\,cm^{-1}$ and corresponding parasitic mid-IR transitions of the RE ions. The underlying effect is a Förster resonance energy transfer (FRET) from excited RE ions to multi-phonon states of the SiO₂ host glass [7,8]. Consequently, VIS fiber lasers with their potential advantages such as high gain, excellent beam quality or good thermal management cannot address applications in bio-medicine, lightning and display technology, material processing or fundamental research, so far.

As a solution, a doping with RE doped nanocrystals (NCs) has been proposed [9]: by proper material selection, such NCs would offer a low phonon energy environment for the RE ions. Besides a RE doping, which is at the focus here, fibers can also contain NCs doped with transition-metal ions [10] or undoped NCs that act as quantum dots [11]. For the actual NC doping of the fibers, two general strategies have been followed, so far. Ex-situ fabricated NCs can either be doped into the so-called preform, which is then drawn into a fiber [12], or the NCs can be grown in-situ in the fiber after drawing by thermal post-processing and nucleation [13]. Fibers fabricated via the latter approach are called glass-ceramic (GC) fibers. Attempts to in-situ

grow the NCs during preform fabrication via phase separation effects [14] can be understood as a variation thereof. So far, the vast majority of reported NC doped fibers were GC fibers, an assessment that can also be found in recent reviews [15–17]. Reasons for this are manifold, but a major issue related to the doping of ex-situ fabricated NCs is the dissolution of almost all NC materials due to the harsh preform fabrication and fiber drawing conditions at temperatures up to 2000°C. Indeed, the in-situ NC growing of GC fibers overcomes this issue but it suffers from a low control with respect to the NC design and RE doping profile. For example, it remains unclear how such in-situ grown NCs can provide undoped shielding shells, as they are common in state-of-the-art ex-situ fabricated NCs [18–21].

If the refractive index of the NCs is not matched to the SiO_2 host glass, undesired Rayleigh scattering defines a maximum tolerable NC size, which must be well below the light wavelength [22]. Obviously, for such small NCs, the multi-phonon quenching cannot be suppressed completely. However, the following question occurs, which has to the best of our knowledge not been addressed before: how is the multi-phonon quenching related to the properties of the SiO_2 host glass and how can it be effectively suppressed by proper material design (purity, dopants etc.) of the SiO_2 glass?

So far, the multi-phonon quenching in NCs has mainly been modelled as a loss process controlled by parameters phenomenologically extracted from or fitted to experimental data [23–25]. Thereby, it is not possible to understand the relevance and interplay of the individual parameters or to identify strategies for efficient suppression of the quenching. Here, a novel analytical model of the FRET interaction of RE doped NCs with the host glass will be presented, which overcomes these issues. Particularly, it will be shown that the multi-phonon quenching depends only on a few macroscopic and experimentally accessible parameters. It will be demonstrated that only if the quality (mid-IR absorption) of the SiO_2 host glass is comparable to ultra-pure SiO_2, the penetration depth of the multi-phonon quenching can be kept at reasonable levels and low lifetime quenching can be expected for sufficiently small NCs. Particularly, this indicates that borosilicate glasses, as have been mainly used as host glasses in GC fibers until now [17], and phosphosilicate glasses are not a good choice. In contrast, arguments will be presented that aluminosilicate glasses are ideal hosts for SiO_2 fibers doped with NCs.

2. Modeling

Assume a RE ion embedded in a NC, for example a crystalline fluoride material such as $LiYF_4$, which is surrounded by a glass host. Since the focus here is on the FRET interaction of the RE ion with the host glass, other effects related the finite NC size (migration, concentration quenching etc.) are not considered hereafter [26]. For example, a potential enhancement of the multi-phonon quenching into the NC itself is neglected because experimental and theoretical data indicate that the phonon spectra of the NCs are only modified in small NCs below 10 nm [27,28]. Note that the majority of the effects not considered here tend to reduce the RE ion lifetime(s) even more than by multi-phonon quenching into the host glass. Thus, the model presented here can be understood as a best-case assessment, but the limitations identified with it cannot be overcome even if all other issues are solved.

During the FRET process, the RE ion, pumped to an excited electronic state, can transfer its energy via a dipole-dipole interaction to the molecular network of the glass, see Fig. 1. It can do so either by excitation of electronic or vibrational states of the molecular lattice. Since the relevant RE transition energies (wavelengths of 2 μm to 4 μm) are well below the SiO_2 bandgap of 8.9 eV and above the SiO_2 phonon energy of around 1100 cm^{-1}, the discussion can be restricted to overtones of lattice vibrations, i.e. multi-phonon transitions. Note that the FRET dipole-dipole interaction should not be confused with a Dexter process because there is no physical electron transfer from the RE ion into the molecular glass structure.
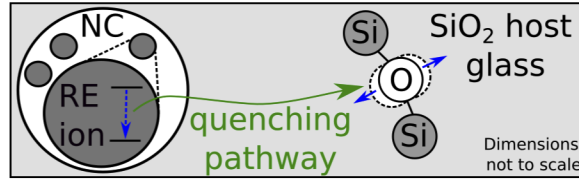
Fig. 1. An excited RE ion inside a NC transfers its energy via a dipole-dipole Förster interaction to the surrounding SiO_2 host glass. A lattice overtone vibration, represented as a vibrating oxygen atom, is induced and the RE ion decays from the excited to a lower electronic state. Thereby, the lifetime of the excited state is quenched.

The rate equation of the upper state population probability $n(t)$ is

$$\frac{d}{dt}n(t) = -\frac{1}{\tau}n - \kappa n + \text{rates of other processes.} \tag{1}$$

τ is the (unquenched) radiative lifetime, which depends on the NC material, and κ is a rate associated with the FRET process. Further processes such as pumping from the ground state or stimulated emission are of no relevance for the following discussions. One can define an effective lifetime τ_{eff} with

$$\frac{1}{\tau_{\text{eff}}} = \frac{1}{\tau} + \kappa \tag{2}$$

and introduce a measure

$$\eta = 1 - \frac{\tau_{\text{eff}}}{\tau} = \frac{\tau\kappa}{1 + \tau\kappa}, \tag{3}$$

which is the quenching factor of the radiative lifetime. For example, $\eta = 0.5$ corresponds to $\kappa = 1/\tau$ and a quenching of 50%.

κ can be computed via Fermi's Golden Law. For a single pair of donor (the RE ion) and acceptor (multi-phonon state) spatially separated by R_{DA}, κ is [29]

$$\kappa = \frac{1}{\tau}\frac{R_0^6}{R_{\text{DA}}^6} \tag{4}$$

with critical radius

$$R_0^6 = \frac{3c\tau}{8\pi^4 n_0^2}\int d\lambda\, \sigma_{\text{em}}^D(\lambda)\sigma_{\text{abs}}^A(\lambda). \tag{5}$$

$\sigma_{\text{em}}^D(\lambda)$ and $\sigma_{\text{abs}}^A(\lambda)$ are the emission and absorption cross section of the donor and the acceptor and c the speed of light. n_0 is the refractive index of the material in-between the donor and acceptor, which is assumed to be constant over the whole overlap integral in Eq. (5). Given the $1/R^6$ scaling of κ, it seems reasonable to assume that n_0 is determined by the refractive index of the NC. Indeed, if the NC and the glass host have similar refractive indices, the choice of n_0 has only a marginal relevance. The following discussions could be performed for any NC shape, but for a spherical NC with radius r_{NC}, analytical results can be found.

For now, assume that the RE ion is embedded at the NC center since the corresponding results are useful for the general case of arbitrary position, which will be discussed later. The FRET rate

is

$$\kappa = \frac{R_0^6}{\tau} \int d^3 r \frac{1}{|\vec{r}|^6} \Theta(|\vec{r}| - r_{\text{NC}}) \rho(\vec{r}) \tag{6}$$

with step-function $\Theta(x) = 0$ for $x < 0$ and $= 1$ for $x > 0$ and acceptor density $\rho(\vec{r})$, which can be assumed to be constant $\rho(\vec{r}) = \rho_0$. By using spherical coordinates it follows that

$$\kappa = \frac{\rho_0}{\tau} R_0^6 4\pi^2 \int_{r_{\text{NC}}}^{\infty} dr \frac{1}{r^4} = \frac{\rho_0}{\tau} \frac{R_0^6}{r_{\text{NC}}^6} V_{\text{NC}} \tag{7}$$

with NC volume $V_{\text{NC}} = 4/3\pi r_{\text{NC}}^3$. Substitution of Eq. (5) yields

$$\kappa = \frac{V_{\text{NC}}}{r_{\text{NC}}^6} \frac{3c}{8\pi^4 n_0^2} \int d\lambda \sigma_{\text{em}}^D(\lambda) \alpha(\lambda) \tag{8}$$

where $\alpha(\lambda) = \sigma_{\text{abs}}^A(\lambda)\rho_0$ is the absorption (in units 1/m) of the glass host. Since the emission cross sections are relatively narrow in crystalline hosts, $\alpha(\lambda) \approx \text{const} = \alpha(\lambda_0) = \alpha_0$ (λ_0 being the center wavelength of the RE transition) in the integral and

$$\kappa = \frac{V_{\text{NC}}}{r_{\text{NC}}^6} \frac{3c\alpha_0}{8\pi^4 n_0^2} \int d\lambda \sigma_{\text{em}}^D(\lambda). \tag{9}$$

Similar results have already been reported before [7,8] in the context of multi-phonon quenching of RE ions doped in pure glass. To simplify Eq. (9) further, one can use that, for an optical transition with transition energy E, the Einstein coefficient $A = 1/\tau$ is related to the emission cross section as [30]

$$\sigma_{\text{em}}(\omega) = A \left(\frac{\pi c}{\omega n_0}\right)^2 g(\omega) \tag{10}$$

with angular frequency $\omega = E/\hbar$. $g(\omega)$ is a normalized lineshape function such that $\int d\omega g(\omega) = 1$. Rearranging and integration with substitution $\omega = 2\pi c/\lambda$ yields

$$A = 8\pi n_0^2 c \int d\lambda \frac{\sigma_{\text{em}}(\lambda)}{\lambda^4}. \tag{11}$$

Since the emission cross sections are relatively narrow, which means $\lambda \approx \text{const} = \lambda_0$ in the integral, it follows that

$$\int d\lambda \sigma_{\text{em}}(\lambda) = \frac{1}{\tau} \frac{\lambda_0^4}{8\pi n_0^2 c}, \tag{12}$$

which is a variation of the Füchtbauer–Ladenburg equation [31]. Substitution in Eq. (9) finally yields

$$\kappa = \frac{1}{\tau} \frac{\alpha_0}{r_{\text{NC}}^3} \left(\frac{\lambda_0}{2\pi n_0}\right)^4 \tag{13}$$

which is an very simple result because the FRET rate κ (of the central RE ion) depends only on the NC size r_{NC}, the (unquenched) radiative lifetime τ, the NC refractive index n_0 (at the transition wavelength), and the host absorption α_0 (at the transition wavelength). With respect to the underlying physics, Eq. (13) is consisting since it involves all parameters expected to be relevant.

In the following, the RE ion is assumed to be at arbitrary position within the NC. Without loss of generality and due to the spherical NC symmetry, one can define a Cartesian coordinate

system such that the RE ion is at position $\mathbf{z} = (0, 0, z)$ where z is the spatial separation from the NC center. The distance $R(z, \mathbf{r})$ to any other point in space $\mathbf{r} = (r, \theta, \phi)$ is

$$R(z, \mathbf{r}) = ||\mathbf{r} - \mathbf{z}||_2 = \sqrt{r^2 - 2rz\cos(\theta) + z^2}. \tag{14}$$

Thus, the position-dependent FRET rate is

$$\kappa(z) = \frac{R_0^6 \rho_0}{\tau} \int_{r_{\text{NC}}}^{\infty} dr \int_0^{\pi} d\theta \int_0^{2\pi} d\phi \frac{r^2 \sin(\theta)}{R^6(z, \mathbf{r})}. \tag{15}$$

Following the same strategy as before for the central RE ion, it follows that

$$\kappa(z) = \frac{3\alpha_0 \lambda_0^4}{\tau 64\pi^5 n_0^4} I(z) \tag{16}$$

with

$$I(z) = 2\pi \int_{r_{\text{NC}}}^{\infty} dr \int_0^{\pi} d\theta \frac{r^2 \sin(\theta)}{\sqrt{r^2 - 2rz\cos(\theta) + z^2}^6}. \tag{17}$$

The integration over θ can be carried out by substitution $u = \sqrt{r^2 - 2zr\cos(\theta) + z^2}$. Using

$$\frac{du}{d\theta} = \frac{zr}{u} \sin(\theta) \tag{18}$$

it follows that

$$I(z) = \frac{2\pi}{z} \int_{r_{\text{NC}}}^{\infty} dr r \int_{r-z}^{r+z} du \frac{1}{u^5} = \frac{2\pi}{4z} \int_{r_{\text{NC}}}^{\infty} dr r \left(\frac{1}{(r-z)^4} - \frac{1}{(r+z)^4} \right) = \frac{4\pi r_{\text{NC}}^3}{3 \left(r_{\text{NC}}^2 - z^2 \right)^3}. \tag{19}$$

Substitution in Eq. (16) finally yields

$$\kappa(z) = \frac{\alpha_0}{\tau} \left(\frac{\lambda_0}{2\pi n_0} \right)^4 \frac{r_{\text{NC}}^3}{\left(r_{\text{NC}}^2 - z^2 \right)^3}, \tag{20}$$

which is an analytical solution for the position-dependent quenching rate inside the NC. To confirm its validity it was successfully checked that numerical triple integration of Eq. (15) yields the same results. Furthermore, for $z = 0$ (RE ion at NC center) Eq. (20) is identical to Eq. (13). In addition, in the context of FRET assisted quenching of NCs into the molecules of a surrounding solvent host, an analytical formula has been presented for the position-dependent quenching rate, see Eq. (2) in [25], which is quite similar to Eq. (15). However, the formula presented in [25] requires a parameter related to the "FRET energy transfer strength" of a single donor acceptor pair, which cannot directly be measured experimentally. In contrast, the result obtained here is directly related to measurable and known parameters such as the absorption.

Based on Eq. (20), the position-dependent quenching factor

$$\eta(z) = \left(1 + \frac{1}{\alpha_0 r_{\text{NC}}^3} \left(\frac{2\pi n_0}{\lambda_0} \right)^4 \left(r_{\text{NC}}^2 - z^2 \right)^3 \right)^{-1} \tag{21}$$

can be computed. The average quenching factor

$$\bar{\eta} = V_{\text{NC}}^{-1} \int_{V_{\text{NC}}} dz d\phi d\theta \, \eta(z) \tag{22}$$

can be expressed conveniently using the dimensionless substitution $q = z/r_{NC}$

$$\bar{\eta} = 3 \int_0^1 dq \frac{q^2}{1 + \chi \left(1 - q^2\right)^3} \tag{23}$$

with the dimensionless parameter

$$\chi = \frac{r_{NC}^3}{\alpha_0} \left(\frac{2\pi n_0}{\lambda_0}\right)^4. \tag{24}$$

To the best of our knowledge, the remaining integral in Eq. (23) cannot be solved analytically. However, it can easily be computed numerically if all relevant design parameters (NC size r_{NC}, transition wavelength λ_0, host absorption α_0 and NC refractive index n_0) are specified through the dimensionless parameter χ.

3. Results

It will be discussed below that the relevant RE ion transition wavelength regime spans from around 2 μm to around 4 μm. If the SiO$_2$ glass is of high purity, its absorption in this regime is mainly given by the multi-phonon absorption tail. However, potential impurities such as hydroxyl groups or dopants are known to increase the absorption, in particular at wavelengths around 3 μm [32,33]. The relevance of this effect will be discussed further below. The SiO$_2$ multi-phonon loss obeys the following general rule [34]

$$\alpha(\lambda) = A_0 \exp(-a/\lambda) \tag{25}$$

where a can computed from fundamental parameters for single component dielectrics [35] and $a \approx 50 \, \mu$m for SiO$_2$. A_0 has been chosen such that the absorption is 20 dB/km (around 8.5×10^4 dB/km) at a wavelength of 2 μm (3 μm), which coincides with the theoretical limit of the SiO$_2$ multi-phonon absorption tail [36] and matches experimental data of ultra-pure SiO$_2$ [37]. The absorption obtained by these numbers is referenced as the best-case scenario in the following. LiYF$_4$ has been assumed as NC material and the corresponding refractive index n_0 has been modelled by Sellmeier coefficients [38]. As a material, LiYF$_4$ is promising because its refractive index matches that of SiO$_2$ quite well, which promises low scattering losses related to the NC doping.

For the best-case SiO$_2$ absorption scenario, Fig. 2 shows the average quenching rate $\bar{\eta}$ in dependency of the transition wavelength λ_0 and the NC diameter $2r_{NC}$ as computed with Eq. (23). As expected, with increasing transition wavelength, increasingly large NCs are required to shield the RE ions from quenching and to maintain a certain level of average quenching. For example, for a transition wavelength of around 3 μm a NC diameter of at least 100 nm is required to obtain an average quenching smaller than 0.2. In NCs below 50 nm, even wavelengths as low as 2 μm experience some quenching, which is consistent with the fact that the 2 μm transition of Tm^{3+} is already slightly quenched in pure SiO$_2$ [39]. The wavelength regime (2.4 μm to 2.9 μm) in-between the two dashed lines belongs to two relevant parasitic mid-IR transitions of RE ions in LiYF$_4$, namely the Pr^{3+} $^3P_0 - ^1D_2$ and the Er^{3+} $^4I_{11/2} - ^4I_{13/2}$ transition [40,41]. In the context of VIS light and laser sources, both are of high relevance, see Fig. 3. Pumping the Pr^{3+} $^3P_0$ state gives access to various potential VIS emission lines [41] if the lifetime of the $^3P_0$ state is sufficiently high. Since the parasitic $^3P_0 - ^1D_2$ transition quenches this lifetime, NCs must be sufficiently large to shield this particular transition. Pumping the Er^{3+} $^4I_{11/2}$ state and cross-relaxation processes among the Er^{3+} ions can yield excitation of higher energy states with subsequent emission in the green [23]. Such Er^{3+} up-conversion requires a high lifetime of the Er^{3+} $^4I_{11/2}$ state and, again, NCs must be large enough to shield this particular transition

from parasitic transitions to the Er^{3+} $^4I_{13/2}$ state. Within the relevant wavelength regime (2.4 μm to 2.9 μm), Fig. 2 indicates that for NCs larger than 50 nm (100 nm), the average quenching is smaller than 0.3 (0.2). However, for NCs as small as 10 nm it is already higher than 0.9 in the worst case (wavelength of 2.9 μm).
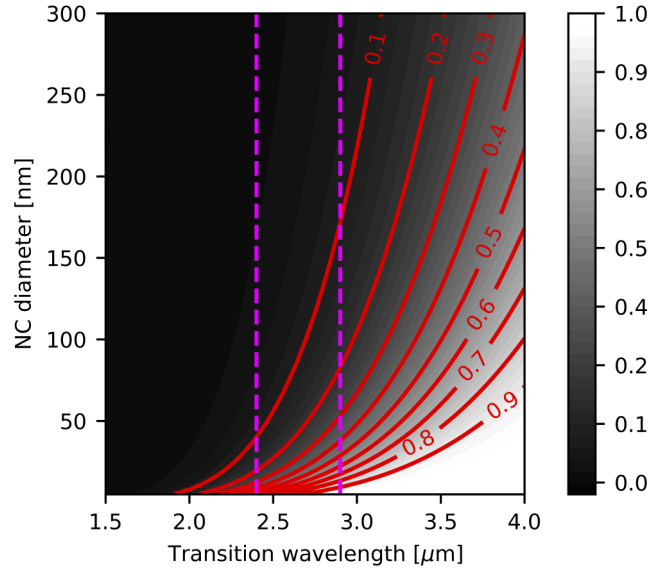

Fig. 2. Average quenching of the RE ions in dependency of the transition wavelength and the NC diameter for the best-case (multi-phonon) SiO_2 absorption case.
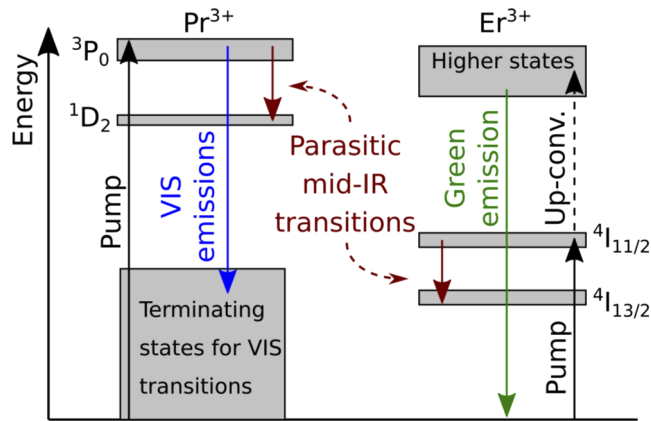

Fig. 3. Schematic diagram of relevant Pr^{3+} (left) and Er^{3+} (right) energy states and transitions (not to scale).

Figure 4 demonstrates how the NC diameter required to maintain a certain level of average quenching, increases if the SiO_2 absorption increases beyond the best-case scenario. A fixed transition wavelength of 2.9 μm was used, which is the upper bound of the transition wavelength regime of the aforementioned parasitic mid-IR Pr^{3+} and Er^{3+} transitions. Interestingly, for each level of average quenching, a tenfold increase of the SiO_2 absorption requires roughly a doubling of the NC diameter to maintain a certain average quenching. For example, for an average quenching of 0.5, the required NC diameter is around 28 nm (best case scenario), around

62 nm for a tenfold increase and around 133 nm for a 100x increase. If the average quenching shall be better than 0.1, the NCs must already be larger than 300 nm for a tenfold increase of the absorption. For a 100x increase, NCs below 100 nm can only maintain an average quenching of around 0.6. For NCs as small as 10 nm and a tenfold increase of the SiO_2 absorption, the average quenching is close to 1, which means the NCs cannot suppress the multi-phonon at all. As discussed above, the quenching for such small NCs is already around 0.9 even for the best-case absorption scenario.
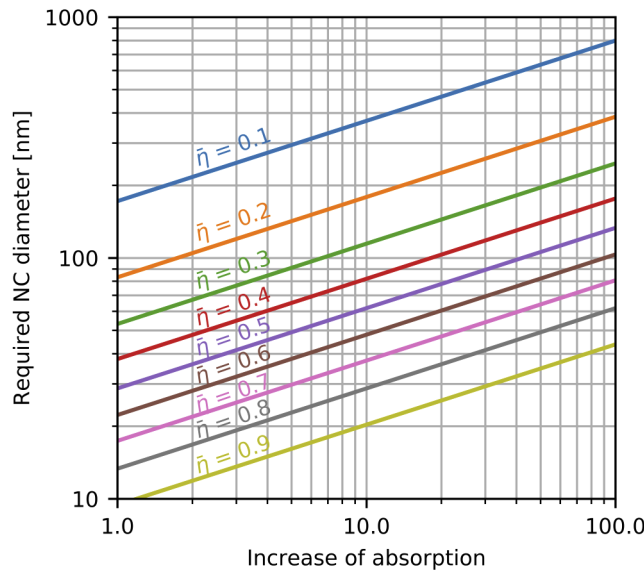

Fig. 4. Minimum required NC diameter for different levels of average quenching in dependency of an increase of the SiO_2 absorption for a fixed transition wavelength of 2.9 μm.

4. Implications regarding the host glass

An increase of the SiO_2 absorption, as it has been assumed, is indeed very likely for two reasons. First, impurities such hydroxyl groups increase the SiO_2 absorption significantly, in particular at the relevant parasitic mid-IR transition wavelengths around 2.4 μm to 2.9 μm [32,33] because the fundamental OH stretching vibrations have energies from around 3700 cm^{-1} (2.7 μm) to around 3500 cm^{-1} (2.9 μm) [42]. For example, it was observed that for a hydroxyl content of less than 0.2 ppm (F300 SiO_2 quality), the mid-IR absorption did not show features related to hydroxyl groups and was close to the best-case absorption scenario as considered above [43]. However, for a hydroxyl content of around 700 ppm (F100 SiO_2 quality) the OH peak absorption increased already by around three orders of magnitude. Similarly, data presented elsewhere [44] can be interpreted such that the hydroxyl peak absorption (in units 1/m) increases roughly by a factor of 1000 if the hydroxyl content (in units ppm) increases by a factor of 10. Other impurities such as transition metal ions or other RE ions are also known to be efficient quenching partners. Consequently, a tenfold increase of the SiO_2 absorption, as assumed above, is indeed a reasonable scenario. Hence, as a first design rule, the SiO_2 host glass should be of highest purity. Common GC fiber fabrication concepts such as the melt-in-tube or molten-core approach do not use glasses derived by vapor-phase processes [17], which typically suffer from a rather low purity. However, counterexamples have also been reported [45]. The results presented here encourage to pay highest attention to the purity of the fiber fabrication process.

The second reason for an increased SiO_2 absorption are dopants as they are commonly used in SiO_2 based fibers to control the refractive index, to enhance the solubility of RE ions or to tailor the required fiber fabrication and processing parameters (e.g. temperature). Such dopants can have a strong impact on the multi-phonon absorption tail by altering the phonon spectrum and the maximum phonon energy. A particular example is a phosphorus doping, which is known to shift the maximum phonon energy to around $1330\,cm^{-1}$ [46]. A corresponding lifetime reduction (increase of the multi-phonon quenching) has for example been observed in Tm^{3+} SiO_2 fibers doped with phosphorus [39]. In $Er^{3+}:Yb^{3+}$ co-doped fibers this effect is even exploited to enhance the Yb^{3+} to Er^{3+} energy transfer [47]. Hence, phosphosilicate glasses cannot be recommended as a basis for NC doped fibers. In this context it is also questionable if borosilicate glasses, as they have been used in many investigations to obtain GC fibers [17], are a good choice. It is known from Raman spectroscopy that the phonon spectra of borosilicate glasses contain high energy bands up to $1500\,cm^{-1}$ [48]. Accordingly, a significant increase of the absorption of boron doped fibers has been observed experimentally [49]. A $5\,wt\%$ B_2O_3 doping increased the mid-IR absorption up to an order of magnitude, indicating again that a tenfold (or even higher) increase of the SiO_2 absorption is a likely scenario. In contrast to phosphosilicate and borosilicate glasses, it has been observed that an aluminum doping yields an increased radiative lifetime of RE ions in SiO_2 [39,50]. In contrast to phosphorus and boron, which increase the maximum phonon energy, aluminum reduces it because, at a molecular level, Si-O-Si bonds are substituted by Al-O-Al bonds, which are known to have a reduced vibrational energy [51]. A corresponding decrease of the mid-IR absorption has been observed in aluminum doped SiO_2 glasses [52] but it remains to be investigated how significant this effect is. Thus, as a second design rule, the SiO_2 host glass should not contain any dopants such as phosphorus or boron that increase the multi-phonon absorption. In contrast, the aluminum doping of aluminosilicate glasses seems to be a promising strategy to reduce the penetration of the multi-phonon quenching effect in RE doped NCs.

5. Conclusion

RE doped NCs doped in SiO_2 fibers, e.g. GC fibers, are promising to overcome the strong multi-phonon quenching of vitreous SiO_2. A novel analytical model was used to investigate how the multi-phonon quenching penetrates the NCs depending on the composition and the properties, in particular the mid-IR absorption, of the SiO_2 host glass. Beyond the discussions presented here, the analytical model could also be used if the host is not glass but a different material. In this context, it could also be applied to compute the required shell thickness of ex-situ fabricated NCs as they are commonly used in solvents [18]. Furthermore, the presented analysis is also valid if the RE ion is not embedded in a crystalline but in a vitreous nanoparticle (NP). Historically, such NP doping has been used very successfully to reduce RE ion clustering [53] but it can also yield vitreous local environments with a low phonon energy [54].

Assuming a best-case absorption scenario, in which the SiO_2 mid-IR absorption is given by the multi-phonon absorption tail, it was shown that for the relevant transition wavelength regime from $2.4\,\mu m$ to $2.9\,\mu m$ and NCs diameters between $50\,nm$ and $100\,nm$, the average quenching is less than 0.3. However, for NCs as small as $10\,nm$ it is already as high as 0.9 in the worst case (wavelength of $2.9\,\mu m$). In case of a tenfold increase of the SiO_2 absorption, NCs below $10\,nm$ cannot provide any reduction of the multi-phonon quenching and the average quenching is near to 1.0. In addition, an average quenching of less than 0.5 can only be expected for NCs larger than $60\,nm$.

Such an increase of the SiO_2 mid-IR absorption is indeed a likely scenario. Impurities such as hydroxyl groups or transition metal ions and common dopants such as phosphorus or boron are known to significantly increase the absorption, in particular in the critical wavelength regime around $2.9\,\mu m$. Thus, phosphosilicate and borosilicate glasses with low purity are expected to significantly degrade the performance of RE doped NCs doped in SiO_2 fibers. In

contrast, high-purity aluminosilicate glasses are promising to maintain a sufficiently low level of multi-phonon quenching.

Disclosures. The authors declare no conflicts of interest

Data availability. Data underlying the results presented in this paper are not publicly available at this time but may be obtained from the authors upon reasonable request.

References

1. W. M. Steen, "Laser material processing - an overview," J. Opt. A: Pure Appl. Opt. **5**(4), S3–S7 (2003).
2. N. Davoudzadeh, G. Ducourthial, and B. Spring, "Custom fabrication and mode-locked operation of a femtosecond fiber laser for multiphoton microscopy," Sci. Rep. **9**(1), 4233 (2019).
3. M. J. F. Digonnet, *Rare-earth-doped Fiber Lasers and Amplifiers* (CRC Press, 2001), 3rd ed.
4. M. Steinke, H. Tünnermann, V. Kuhn, T. Theeg, M. Karow, O. de Varona, P. Jahn, P. Booker, J. Neumann, P. Weßels, and D. Kracht, "Single-frequency fiber amplifiers for next-generation gravitational wave detectors," IEEE J. Sel. Top. Quantum. Electron. **24**(3), 1–13 (2018).
5. M.-P. Lord, F. Maes, V. Fortin, M. Bernier, and R. Vallée, "Watt-level visible laser emission in a double-clad praseodymium-doped fluoride fiber," in *Laser Congress 2020 (ASSL, LAC)*, (2020). paper ATh5A.6.
6. I. Cozmuta, S. Cozic, M. Poulain, S. Poulain, and J. R. L. Martini, "Breaking the silica ceiling: ZBLAN-based opportunities for photonics applications," Proc. SPIE **11276**, 112760R (2020).
7. S. A. Payne and C. Bibeau, "Picosecond nonradiative processes in neodymium-doped crystals and glasses: mechanism for the energy gap law," J. Lumin. **79**(3), 143–159 (1998).
8. K. K. Pukhiv, F. Pelle, and J. Heber, "Multiphonon relaxation of excited rare-earth ions in ionic matrices," Mol. Phys. **101**(7), 1001–1006 (2003).
9. P. A. Tick, N. F. Borrelli, L. K. Cornelius, and M. A. Newhouse, "Transparent glass ceramics for 1300 nm amplifier applications," J. Appl. Phys. **78**(11), 6367–6374 (1995).
10. Z. Fang, S. Zheng, W. Peng, H. Zhang, Z. Ma, G. Dong, S. Zhou, D. Chen, and J. Qiu, "Ni^{2+} doped glass ceramic fiber fabricated by melt-in-tube method and successive heat treatment," Opt. Express **23**(22), 28258–28263 (2015).
11. Z. Peng, X. Huang, Z. Ma, G. Dong, and J. Qiu, "Surface modification and fabrication of white-light-emitting Tm^{3+}/CdS quantum dots co-doped glass fibers," J. Am. Ceram. Soc. **102**(10), 5818–5827 (2019).
12. C. C. Baker, E. J. Friebele, A. A. Burdett, D. L. Rhonehouse, A. Fontana, W. Kim, S. R. Bowman, L. B. Shaw, J. Sanghera, J. Zhang, R. Pattnaik, M. Dubinskii, J. Ballato, C. Kucera, A. Vargas, A. Hemming, N. Simakov, and J. Haub, "Nanoparticle doping for high power fiber lasers at eye-safer wavelengths," Opt. Express **25**(12), 13903–13915 (2017).
13. B. N. Samson, P. A. Tick, and N. F. Borrelli, "Efficient neodymium-doped glass-ceramic fiber laser and amplifier," Opt. Lett. **26**(3), 145–147 (2001).
14. A. V. Kiryanov, M. Paul, Y. O. Barmenkov, S. Das, M. Pal, S. K. Bhadra, L. E. Zarate, and A. D. Guzman-Chavez, "Fabrication and characterization of new Yb-doped zirconia-germano-alumino silicate phase-separated nano-particles based fibers," Opt. Express **19**(16), 14823–14837 (2011).
15. J. Ballato, H. Ebendorff-Heidepriem, J. Zhao, L. Petit, and J. Troles, "Glass and process development for the next generation of optical fibers: a review," Fibers **5**(1), 11 (2017).
16. A. Veber, Z. Lu, M. Vermillac, F. Pigeonneau, W. Blanc, and L. Petit, "Nano-structured optical fibers made of glass-ceramics, and phase separated and metallic particle-containing glasses," Fibers **7**(12), 105 (2019).
17. S. Kang, G. Dong, J. Qiu, and Z. Yang, "Hybrid glass optical fibers - novel fiber materials for optoelectronic application," Opt. Mater. **6**, 100051 (2020).
18. F. Carl, L. Birk, B. Grauel, M. Pons, C. Würth, U. Resch-Genger, and M. Haase, "LiYF$_4$:Yb/LiYF$_4$ and LiYF$_4$:Yb, Er/LiYF$_4$ core/shell nanocrystals with luminescence decay times similar to YLF laser crystals and the upconversion quantum yield of the Yb, Er doped nanocrystals," Nano Res. **14**(3), 797–806 (2021).
19. A. Skripka, A. Benayas, C. D. S. Brites, I. R. Martín, L. D. Carlos, and F. Vetrone, "Inert shell effect on the quantum yield of Neodymium-doped near-infrared nanoparticles: the necessary shield in an aqueous dispersion," Nano Lett. **20**(10), 7648–7654 (2020).
20. C. Siefe, R. D. Mehlenbacher, C. S. Peng, Y. Zhang, S. Fischer, A. Lay, C. A. McLellan, A. P. Alivisatos, S. Chu, and J. A. Dionne, "Sub-20 nm core–shell–shell nanoparticles for bright upconversion and enhanced Förster resonant energy transfer," J. Am. Chem. Soc. **141**(42), 16997–17005 (2019).
21. S. Fischer, N. D. Bronstein, J. K. Swabeck, E. M. Chan, and A. P. Alivisatos, "Precise tuning of surface quenching for luminescence enhancement in core–shell lanthanide-doped nanocrystals," Nano Lett. **16**(11), 7241–7247 (2016).
22. P. A. Tick, "Are low-loss glass-ceramic optical waveguides possible?" Opt. Lett. **23**(24), 1904–1905 (1998).
23. S. Fischer, H. Steinkemper, P. Löper, M. Hermle, and J. C. Goldschmidt, "Modeling upconversion of erbium doped microcrystals based on experimentally determined Einstein coefficients," J. Appl. Phys. **111**(1), 013109 (2012).

24. P. Villanueva-Delgado, K. W. Krämer, and R. Valiente, "Simulating energy transfer and upconversion in β-NaYF$_4$: Yb^{3+}, Tm^{3+}," J. Phys. Chem. C **119**(41), 23648–23657 (2015).

25. F. T. Rabouw, P. T. Prins, P. Villanueva-Delgado, M. Castelijns, R. G. Geitenbeek, and A. Meijerink, "Quenching pathways in NaYF$_4$:Er^{3+}, Yb^{3+} upconversion nanocrystals," ACS Nano **12**(5), 4812–4823 (2018).

26. J. Collins, "Non-radiative processes in crystals and in nanocrystals," ECS J. Solid State Sci. Technol. **5**(1), R3170–R3184 (2016).

27. Z. H. Li, D. Hudry, R. Heid, A. H. Said, M. D. Le, R. Popescu, D. Gerthsen, M. Merz, K. W. Krämer, D. Busko, I. A. Howard, B. S. Richards, and F. Weber, "Phonon density of states in lanthanide-based nanocrystals," Phys. Rev. B **102**(16), 165409 (2020).

28. S. Osswald, V. N. Mochalin, M. Havel, G. Yushin, and Y. Gogotsi, "Phonon confinement effects in the Raman spectrum of nanodiamond," Phys. Rev. B **80**(7), 075419 (2009).

29. J. L. Philipsen and A. Bjarklev, "Monte Carlo simulations of homogeneous upconversion in erbium-doped silica glasses," IEEE J. Quantum Electron. **33**(5), 845–854 (1997).

30. R. C. Hilborn, "Einstein coefficients, cross sections, f values, dipole moments, and all that," Am. J. Phys. **50**(11), 982–986 (1982).

31. B. F. Aull and H. P. Jenssen, "Vibronic interactions in Nd:YAG resulting in nonreciprocity of absorption and stimulated emission cross sections," IEEE J. Quantum Electron. **18**(5), 925–930 (1982).

32. F. Nürnberg, B. Kühn, A. Langner, M. Altwein, G. Schötz, R. Takke, S. Thomas, and J. Vydra, "Bulk damage and absorption in fused silica due to high-power laser applications," in *Laser-Induced Damage in Optical Materials: 2015*, vol. 9632 (SPIE, 2015), pp. 354–363.

33. C. R. Elliott and G. R. Newns, "Near infrared absorption spectra of silica: OH overtones," Appl. Spectrosc. **25**(3), 378–379 (1971).

34. J. Sanghera and I. D. Aggarwal, *Infrared Fiber Optics* (CRC Press, 1998).

35. M. Lines, "Theoretical limits of low optic loss in multicomponent halide glass materials," J. Non-Cryst. Solids **103**(2-3), 265–278 (1988).

36. F. Nürnberg, B. Kühn, and K. Rollmann, "Metrology of fused silica," in *Laser-Induced Damage in Optical Materials 2016*, vol. 10014 (SPIE, 2016), pp. 42–54.

37. T. J. Moore and M. R. Jones, "Experimental measurements of the spectral absorption coefficient of pure fused silica optical fibers," Appl. Opt. **54**(6), 1374–1378 (2015).

38. N. P. Barnes and D. J. Gettemy, "Temperature variation of the refractive indices of yttrium lithium fluoride," J. Opt. Soc. Am. **70**(10), 1244–1247 (1980).

39. B. Faure, W. Blanc, B. Dussardier, and G. Monnom, "Improvement of the Tm^{3+}:^{3}H$_4$ level lifetime in silica optical fibers by lowering the local phonon energy," J. Non-Cryst. Solids **353**(29), 2767–2773 (2007).

40. M. R. Brown, K. G. Roots, and W. A. Shand, "Energy levels of Er^{3+} in LiYF$_4$," J. Phys. C: Solid State Phys. **2**(4), 593–602 (1969).

41. L. Esterowitz, F. J. Bartoli, R. E. Allen, D. E. Wortman, C. A. Morrison, and R. P. Leavitt, "Energy levels and line intensities of Pr^{3+} in LiYF$_4$," Phys. Rev. B **19**(12), 6442–6455 (1979).

42. J. Stone and G. E. Walrafen, "Overtone vibrations of OH groups in fused silica optical fibers," J. Chem. Phys. **76**(4), 1712–1722 (1982).

43. O. Humbach, H. Fabian, U. Grzesik, U. Haken, and W. Heitmann, "Analysis of OH absorption bands in synthetic silica," J. Non-Cryst. Solids **203**, 19–26 (1996).

44. V. G. Plotnichenko, V. O. Sokolov, and E. M. Dianov, "Hydroxyl groups in high-purity silica glass," Inorg. Mater. **36**(4), 404–410 (2000).

45. S. Shibata, S. Mitachi, and S. Takahashi, "High numerical aperture multicomponent glass fiber," Appl. Opt. **19**(9), 1484–1488 (1980).

46. V. Plotnichenko, V. Sokolov, V. Koltashev, and E. Dianov, "On the structure of phosphosilicate glasses," J. Non-Cryst. Solids **306**(3), 209–226 (2002).

47. V. P. Gapontsev, S. M. Matitsin, A. A. Isineev, and V. B. Kravchenko, "Erbium glass lasers and their applications," Opt. Laser Technol. **14**(4), 189–196 (1982).

48. A. K. Yadav and P. Singh, "A review of the structures of oxide glasses by Raman spectroscopy," RSC Adv. **5**(83), 67583–67609 (2015).

49. T. Izawa, N. Shibata, and A. Takeda, "Optical attenuation in pure and doped fused silica in the IR wavelength region," Appl. Phys. Lett. **31**(1), 33–35 (1977).

50. J. Cajzl, P. Peterka, M. Kowalczyk, J. Tarka, G. Sobon, J. Sotor, J. Aubrecht, P. Honzátko, and I. Kašík, "Thulium-doped silica fibers with enhanced fluorescence lifetime and their application in ultrafast fiber lasers," Fibers **6**(3), 66 (2018).

51. R. M. Nor, S. N. M. Halim, M. F. M. Taib, A. B. M. A. Ibrahim, and M. K. Abd-Rahman, "First principles study on phonon energy in SiO$_2$ glass with the incorporation of Al$_2$O$_3$," in *Solid State Science and Technology XXIX*, vol. 268 of *Solid State Phenomena* (Trans Tech Publications Ltd, 2017), pp. 160–164.

52. Y. Ohmori, T. Miya, and M. Horiguchi, "Transmission-loss characteristics of Al$_2$O$_3$-doped silica fibers," J. Lightwave Technol. **1**(1), 50–56 (1983).

53. J. J. Koponen, L. C. Petit, T. Kokki, V. Aallos, J. Paul, and H. Ihalainen, "Progress in direct nanoparticle deposition for the development of the next generation fiber lasers," Opt. Eng. **50**(11), 111605 (2011).

54. M. Vermillac, H. Fneich, J.-F. Lupi, J.-B. Tissot, C. Kucera, P. Vennéguès, A. Mehdi, D. R. Neuville, J. Ballato, and W. Blanc, "Use of Thulium-doped LaF$_3$ nanoparticles to lower the phonon energy of the thulium's environment in silica-based optical fibres," Opt. Mater. **68**, 24–28 (2017).